Apr 3rd, 12:00 AM

Ground Testing of High Chamber-Pressure Propulsion Systems

A. W. Langill
Engineering Supervisor, Aerojet-General Corporation

GROUND TESTING OF HIGH CHAMBER-PRESSURE PROPULSION SYSTEMS

A. W. Langill, Jr.
Engineering Supervisor
Aerojet-General Corporation
Sacramento, California

This paper describes the analysis, design and mechanization of a ground support system for application during the captive testing of high chamber-pressure propulsion systems and components. A dual-piston intensifier concept is employed to transform pneumatic control pressures into corresponding propellant supply pressures at the inlet to the thrust chamber assembly under test; a mechanical pressure amplification ratio of over 5 to 1 is achieved in the intensifier design. High speed gas pressurization valves are servo controlled to establish and maintain the desired propellant feed pressures during both transient and steady-state TCA operational phases. Transient control has been satisfactorily implemented at pressure rise rates of up to 10,000 psi/second.

Introduction

The mechanical intensifier assembly can be characterized as a dual-piston pressure amplification device, capable of transforming a relatively low pressure gas driving medium into a corresponding high pressure propellant supply. The intensifier assemblies illustrated in Figs. (1) and (2) were designed to generate propellant pressures of over 6000 psi; because of the 5.2:1 design piston area ratio, the corresponding inlet gas pressure required was slightly less than 1200 psi. Hence, the intensifier concept provides the high pressure propellant environment necessary for the static testing of high-Pc propulsion systems, but eliminates the need for expensive high pressure propellant tankage and gas reservoir capabilities.

Both fuel and oxidizer intensifiers of Figs. (1) and (2) were identical in design; the dual-piston assembly stroke was approximately 110 inches, while the gas and liquid side cavity volumes were 622 and 120 gallons respectively. Although storable propellants were involved in the test program described in this paper, the intensifier concept applies also to cryogenic and advanced slurry-type propellants.

The test hardware (not shown in Figs. 1 or 2) consisted of a dual combustor thrust chamber assembly (TCA). In the final engine configuration, the primary combustor functions as an oxidizer rich gas generator, the exhaust gases from which drive an integral turbopump assembly. Turbine exhaust gases react with additional fuel in the secondary combustor.

For purposes of thrust chamber assembly testing, the pressure intensifier output supply was employed to simulate the engine pump start characteristics. In particular, thrust chamber assembly primary combustor ignition occurs at a low pressure level; this is then followed by a rapid increase to the desired operating pressure level. In order to simulate actual engine operation, it was thus necessary to consider variations in the intensifier outlet pressures as predetermined functions of time.

To establish and maintain the transient intensifier outlet pressures, a form of automatic control system was required. Since the principal control system objective was that of maintaining the intensifier propellant discharge pressure (or equivalently, the TCA inlet pressure), a direct propellant pressure feedback control mode would be an obvious approach. However, due to the short TCA firing duration (approximately 3 seconds total run time) a reasonable degree of control could be attained only through the design of a high frequency response servo system. If propellant pressure were sensed as the feedback parameter, the high-mass intensifier piston would then become a component in the closed loop, and the resulting transient response would be greatly lowered. Because of this consideration, a gas-cavity pressure control mode was selected; i.e. flow valves, located between the intensifier and the source of pressurization gas were modulated so as to establish and maintain the desired intensifier gas-cavity pressures.

At the Aerojet-General Corporation, automatic servo control systems are employed extensively in the testing of liquid rocket propulsion systems and subsystems[1]. The typical servo system "building block," illustrated in Fig. (3), can be characterized in terms of a multi-loop electro-hydraulic system capable of accurately transforming a low-power electrical input excitation into a corresponding high-power mechanical output. In particular, an electrical "set-point" voltage is impressed across the command terminals of an Aerojet-designed servo controller. The servo controller drives a standard servo valve that is hydraulically coupled to a flow control valve. Control valve position feedback is employed to stabilize the inner loop components against gain or dynamical variations. Control valve modulation produces, through the system dynamics, changes in the downstream parameters of interest (e.g. fluid temperature, pressure, flow rate, etc.). The appropriate downstream variable (controlled variable) is sensed with an applicable transducer; the electrical transducer output provides the primary source of degenerative feedback and thus is used to close the loop. In the present application, the controlled variable of interest was the intensifier gas-cavity pressure level.

Servo System Design

Due to the nonlinearities involved in the intensifier and associated test stand support systems (square-law relationships between flow rate and pressure drop, volumes varying as a function of flow rates, nonlinear valve characteristics, etc.) an analytical design was not practical, except in a very preliminary and approximate sense. Rather, the analog computer was used to solve the nonlinear mathematical model; an analogy was thus established between the "machine variable"--voltage--and the physical system variables of interest--bottle pressure, gas flow rate, valve C_v,

volume, etc. At any point in the simulation, the machine voltages could be equated to corresponding test stand and engine variables, i.e. the computer voltages vary during a simulated engine test in the same way that the analogous engine and test stand parameters vary.

Using the computer-design procedure, the overall system mathematical model was first developed and all constants and parameters required in the mathematical model determined, either experimentally or analytically. A "program" was then prepared--the program is a particular arrangement of analog computer components (potentiometers, amplifiers, function generators, multipliers, etc.) such that the correct analogy is established between the program and the engine and test stand system. The program was verified by means of an analytically computed static voltage check. Only after the system had been programmed, all parameters evaluated and potentiometers set, and the static check solution completed satisfactorily could the system design be initiated. The final step in the computer simulation was that of applying the design to a large number of possible test stand conditions.

Fig. (4) illustrates the functional diagram that was considered for computer simulation. The gas system, shown to the left of Fig. (4), begins with the gas storage bottles (P_{gBO} and P_{gBF}). Lines leading from the gas bottles to the fuel and oxidizer gas flow control valves are approximated as lumped resistances and volumes (with line pressures of P_{gLO} and P_{gLF}), together with acceleration effects. Instantaneous gas (GN_2) flow rates are illustrated as $\dot{w}_{gBO}$ and $\dot{w}_{gBF}$ from the oxidizer and fuel bottles respectively. Due to line capacitance effects, the flow rates will not, in the dynamic mode, be equal to the control valve flow rate $\dot{w}_{PRVO}$ and $\dot{w}_{PRVF}$. Symbols P_{gIO} and P_{gIF} represent the oxidizer and fuel booster gas-cavity pressures; the volumes of these equivalent "bottles" vary with piston displacement. The computer was mechanized to permit the simulation of gas bleed valve flow rates, $\dot{w}_{gDO}$ and $\dot{w}_{gDF}$.

The booster dynamics involve a force balance across gas-side and liquid-side pistons. Any force imbalance produces an acceleration of the piston, and hence a changing velocity and position. At the liquid-side piston faces, the piston velocities are proportional to propellant weight flow rates ($\dot{w}_{IO}$ and $\dot{w}_{IF}$). These flow rates now discharge into the remaining liquid-side cavity volumes (indicated by bottles with pressures P_{LIO} and P_{LIF}). Propellant compressibility effects enter into the model at this point, such that the intensifier output flow rates ($\dot{w}_{OL}$ and $\dot{w}_{FL}$) can differ from the flows generated at the pistons.

From the booster outlets, the line flows through the stand plumbing (approximated as bottles with pressure P_{OTCV} and P_{FTCV}), and into the primary and secondary fuel and oxidizer systems. Engine propellant feed systems (to both primary and secondary combustors) are characterized in terms of the flow resistances c_1 through c_{12}, together with the thrust chamber valves and dump valves as shown in Fig. (4). The two feed systems are ultimately "coupled" in terms of primary and secondary chamber pressures.

Fig. (5) illustrates the general form of closed loop servo system, adapted to the control of the oxidizer intensifier gas-cavity pressure (P_{gIO}). Note that proportional-plus-integral compensation is employed in order to eliminate all steady-state controlled-variable errors.

The mathematical model illustrated in Appendix I was based upon the functional diagrams of Figs. (4) and (5). All dimensions are in consistent engineering units, e.g., ^{o}R, inches, pounds, psi, lb/sec, lb/ft^3, ft^3, etc.

Analog Computer Program

Typical portions of the analog computer program arising from the simulation of the mathematical model, are illustrated in Figs. (6) through (12). The program was mechanized for simulation using a PACE 231-R and two PACE 131-R analog computers. Variable engine sequencing was included in the program such that valve actuation timing could be easily varied. A staged P_{cpc} and P_{csc} capability was also included to simulate the effects introduced at the point of secondary fuel fill, while fill volumes were considered in the chamber pressure equations.

Fig. (6) illustrates the simulation of all oxidizer circuit gas flow equations; the fuel circuit simulation diagram (not shown) was identical in composition to that of Fig. (6). In Fig. (7), the intensifier dynamics and liquid flow characteristics are illustrated; further, the secondary combustor flow dynamics are included. Again, the corresponding fuel side flow circuit simulation was structurally identical and is not included. The oxidizer primary flow simulation is shown in Fig. (8); the fuel diagram was again identical.

Both primary and secondary chamber pressure computations are mechanized for analog computer simulation in Fig. (9). Note that primary and secondary fill volumes are simulated, while the required logic inherent in the thrust chamber operation is included. Fig. (10) illustrates the gas flow control valve simulation, and is symbolically identical to the system of Fig. (5). Ramp generators are required, in the simulation, in order to provide a changing input voltage into the servo sub-systems; the ramp generators were implemented in terms of analog integrators as illustrated. The limiting diodes that appear throughout Fig. (10) are required due to physical control hardware limitations.

Fig. (11) was employed to simulate all on-off TCA thrust chamber valves and system dump and bleed valves. The simulation of individual valves in this manner permitted various TCA start and shutdown sequences to be investigated in conjunction with the pressure and flow rate environment generated by the intensifiers. Fig. (12) illustrates the analog computer logic that was inserted for purposes of valve sequencing.

The principal purpose of the analog computer approach was that of developing an acceptable gas-cavity pressure control system design. As illustrated in Figs. (5) and (10), the design parameters were K_O (general forward loop gain), K_P (proportional gain), K_I (internal gain) and K_2 (inner

loop gain). Based upon previous experience, the inner loop gain was set at 5, while K_P was arbitrarily set at unity such that the total forward loop proportional gain was K_O, while the total integral gain was $K_O K_I$. The two remaining design parameters, K_O and K_I were determined to insure stable operation over a wide range of system conditions (bottle pressure, pre-set levels and booster ullages), and to simultaneously permit a reasonable transient response and limited pressure overshoot.

In order to define an approximate starting point, an analytical stability analysis was conducted, assuming only proportional control. The resulting analysis indicated an electrical loop gain of approximately 100 would produce a stable response. The proportional potentiometers of Fig. (10) were thus adjusted to an initial value of .4000 ($K_O K_P/50$) and a series of simulations were conducted for nominal intensifier gas-cavity ullages and 3000 psi bottle pressures. From this starting point, the proportional gains were varied and integral gains introduced and varied until an optimum system response was achieved. The resulting system was found capable of following a 10,000 psi/second pressure ramp, and providing a suitable period of steady-state pressure operation. Booster gas bleed valves were assumed to be open throughout the entire run duration; this feature minimized the pressure overshoot that occurred at the time of ramp termination.

Approximately 150 computer runs were completed to evaluate the gas-cavity servo design under a variety of environmental conditions. During each of the runs, different combinations of bottle pressures (2000, 2250, 2500, 2750, and 3000 psi), initial piston ullages (5, 10, 15, 20 and 25 inches of piston displacement) and initial liquid pre-pressure levels (750, 500 and 450 psi oxidizer and 500, 250 and 125 psi fuel) were simulated to define the operating window of acceptable control system response.

Control System Mechanization

The physical control system mechanization was accomplished by the programming of an on-line analog processor (EAI PC-12), located in the test complex control room. The PC-12 circuits illustrated in Figs. (13) and (14) were constructed to function in conjunction with the servo sub-system design that was defined during control systems analysis. Note that two flow control valves were required for maintaining intensifier gas-cavity pressures. Due to the large variation in control pressures (from less than 50 psi during primary combustor ignition to over 1200 psi during steady-state), each main gas flow control valve was provided with a small (2-inch) auxiliary by-pass flow control valve. The small valve was sequenced to control during primary chamber ignition; at the initiation of the pressure ramp, however, the large (4-inch) flow control valve assumed command, while the by-pass valve closed automatically.

A variety of malfunction safeguards were also programmed for on-line computer execution. Thus, to prevent hardware or facility damage, an immediate fail-safe shutdown was programmed to occur for a variety of conditions; e.g. if the fuel intensifier gas-cavity pressure exceeded the oxidizer gas-cavity pressure.

The PC-12 malfunction circuits of Fig. (14) were coupled into fail-safe manifolds associated with each flow control valve. The fail-safe manifold is physically inserted between the servo valve and the servo block; in the energized or normal mode, the manifold permits the servo valve to function normally. In the de-energized or fail-safe mode, however, the manifold completely over-rides the servo valve signals and functions to close the associated control valve in some predetermined characteristic time. As long as no malfunction conditions exist (as computed in the on-line processor), the fail-safe manifolds are electrically energized; however, should a malfunction condition occur, the gas-cavity pressurization valves close under controlled (fail-safe) command.

Test Data Analysis

Typical control system response characteristics are illustrated in Figs. (15) and (16) for the oxidizer and fuel intensifier systems respectively. Prior to the programmed pressure rise ramps, the intensifier gas-cavity pressures are maintained through the use of the small by-pass flow control valves. Note that the stability characteristics are excellent; i.e. the gas-cavity pressure fluctuations are insignificant.

At ramp rise initiation, the by-pass flow control valves automatically close, while the large flow control valves assume command. The transient response characteristics of both fuel and oxidizer intensifier pressurization systems are excellent; after an initial lag, the gas-cavity pressure is maintained in accordance with the programmed criteria until ramp termination.

A small pressure overshoot occurs following the ramp termination. This condition is caused by the fact that, throughout the ramp rise, a large gas flow rate is required in order to increase the gas-cavity pressure and simultaneously to compensate for propellant compressibility effects. To maintain the desired "steady-state" gas flow rate throughout the pressure rise ramp, the associated control valve is open further than necessary to maintain gas-cavity pressure during the true steady-state portion of the run. Hence, at the point of ramp termination, the flow control valve position must decrease rapidly. Due to the finite servo loop bandwidth, a slight pressure overshoot occurs as noted. The overshoot is decreased, however, by the process of permitting a 2-inch gas-cavity vent valve to remain open throughout the TCA run.

A total of approximately 40 runs have been conducted using the intensifier control concept illustrated in this paper. Repeatability has been excellent, and the system, as designed, has been capable of generating all pressure rise ramps (up to 10,000 psi/second) desired for TCA development.

The importance of a correct servo system design is graphically illustrated by the static test firing data of Fig. (17). In this instance, the fuel intensifier pressure control system gains were set incorrectly, producing the oscillatory response characteristics as shown. The instability produced in this loop can be easily observed by considering the servo input error voltage; i.e. the error voltage amplitudes increased throughout

the run duration. This test was automatically terminated by a computer originated fail-safe command, preventing any hardware damage.

Conclusions

Based upon the analog computer design study and the results of actual thrust chamber assembly test data, the following conclusions can be documented:

1. The gas-cavity control technique permits the mechanical pressure intensifier to adequately follow pressure ramps on the order of 10,000 psi/second.

2. Based upon a constant multiplication factor of the intensifier piston area ratio, the gas-cavity pressure can be directly related to a corresponding propellant pressure control.

3. Pressure overshoots following the completion of a high rise rate ramp transient are acceptable for the majority of thrust chamber assembly applications.

4. Steady-state operating durations of approximately one second (based upon a nominal three second total run duration) can be achieved at essentially zero control error.

---

[1] Langill, A.W., and H. Friedland, "The Application of Automation in the Captive Testing of Space-Vehicle Propulsion Systems," Record of the 1965 International Space Electronics Symposium, Miami Beach, Florida, 1965

Appendix I
Mathematical Model

1. $$\dot{P}_{gBO} = -\frac{RT}{144\, V_{gBO}}\, \dot{w}_{gBO}$$

2. $$P_{gBO} - P_{gLO} = \frac{C_{O_O}}{\rho_{gO}}\, \dot{w}_{gBO}^2 + \frac{\ell}{gA}\, \ddot{w}_{gBO}$$

3. $$\rho_{gB} = (\rho_{gBO} + \rho_{gLO})/2$$

4. $$\dot{P}_{gLO} = \frac{RT}{144\, V_{gLO}}\, (\dot{w}_{gBO} - \dot{w}_{PRVO})$$

5. $$\dot{w}_{PRVO} = \frac{k}{\sqrt{T_T}}\, P_{gLO}\, C_d a_{PRVO}^N$$

where $C_d a = .0287 C_V$

6. $$W_{gIO} = \left(\frac{28 \text{ lb.}}{358 \text{ ft}^3}\right)\left(\frac{492^\circ R}{540^\circ R}\right)\left(\frac{P_{gIO} \text{ psi}}{14.7 \text{ psi}}\right)\left(V_{gIO} \text{ ft}^3\right)$$

or

$$P_{gIO} = \frac{206\, W_{gIO}}{V_{gIO}}$$

7. $$W_{gIO} = \int_0^t (\dot{w}_{PRVO} - w_{gDO})\, dt$$

8. $$w_{gDO} = \frac{k}{\sqrt{T_T}}\, P_{gIO}\, C_d\, a_{ODV_g}$$

9. $$V_{gIO} = \frac{A_{P_g}}{1728}\, x_{PO} + V_{gIO}\,(O)$$

10. $$\Delta F_O = A_{P_g}\, P_{gIO} - A_{P_L} P_{LIO}$$

$$= \frac{1}{12}\, M_P\, \ddot{x}_{P_O} + B\, \dot{x}_{PO}$$

11. $$\dot{w}_{IO} = \frac{A_{PL}}{1728}\, \rho_O\, \dot{x}_{PO}$$

12. $$\dot{P}_{LIO} = \frac{\beta}{V_{LIO}}\, (\dot{w}_{IO} - \dot{w}_{OL})$$

13. $$V_{LIO} = V_{LIO}\,(\text{Final}) - V_{LIO}\,(O) - \frac{A_{PL}}{1728}\, x_{PO}$$

14. $$P_{LIo} - P_{OTCV} = \frac{C_{1O}}{\rho_O}\, \dot{w}_{OL}^2 + \frac{\ell}{gA}\, \ddot{w}_{OL}$$

15. $$\dot{P}_{OTCV} = \frac{\beta}{V_{OTCV}}\, \dot{w}_{OL} - \dot{w}_{OPC} - \dot{w}_{OSC} - \dot{w}_{OD})$$

16. $$P_{OSTCV} = P_{OTCV} - \frac{C_1}{\rho_O}\, \dot{w}_{OSC}^2$$

17. $$P_{OPTCV} = P_{OTCV} - \frac{C_2}{\rho_O}\, \dot{w}_{OPC} + \dot{w}_{OD})^2$$

18. $$\dot{w}_{OSC} = \frac{C_{V_{OSTCV}}}{56.8}\, \sqrt{\rho_O\, (P_{OSTCV} - P_{OJSC\text{-}U})}$$

19. $$\dot{w}_{OPC} = \frac{C_{V_{OPTCV}}}{56.8}\, \sqrt{\rho_O\, (P_{OPTCV} - P_{OJPC\text{-}U})}$$

20. $$\dot{w}_{OD} = \frac{C_{V_{ODV}}}{56.8}\, \sqrt{\rho_O P_{OPTCV}}$$

21. $$P_{OJSC} = P_{OJSC\text{-}U} - \frac{C_3}{\rho_O}\, \dot{w}_{OSC}^2$$

22. $$P_{OJPC} = P_{OJPC\text{-}U} - \frac{C_4}{\rho_O}\, \dot{w}_{OPC}^2$$

23. $P_{OJSC-U} = P_{SCS} + \frac{C_3 + C_5}{\rho_O} \dot{w}_{OSC}^2$

24. $P_{OJPC-U} = P_{CPC} + \frac{C_4 + C_6}{\rho_O} \dot{w}_{OPC}^2$

25. $\dot{P}_{gBF} = - \frac{RT}{144\ V_{gBF}} \dot{w}_{gBF}$

26. $P_{gBF} - P_{gLF} = \frac{C_{OF}}{\rho_{gF}} \dot{w}_{gBF}^2 + \frac{\ell}{gA} \ddot{w}_{gBF}$

27. $\rho_{gF} = (\rho_{gBF} + \rho_{gLF})/2$

28. $\dot{P}_{gLF} = \frac{RT}{144\ V_{gLF}} (\dot{w}_{gBF} - \dot{w}_{PRVF})$

29. $\dot{w}_{PRV} = \frac{k}{\sqrt{T_T}} P_{gLF}\ C_d a_{PRVF} N$

30. $P_{gIF} = \frac{206\ W_{gIF}}{V_{gIF}}$

31. $W_{gIF} = \int_0^t (\dot{w}_{PRVF} - \dot{w}_{gDF})\ dt$

32. $\dot{w}_{gDF} = \frac{k}{\sqrt{T_T}} P_{gIF}\ C_d\ a_{FDVg}$

33. $V_{gIF} = \frac{A_{Pg}}{1728} x_{PF} + V_{gIF(O)}$

34. $\Delta F_F = A_{Pg}\ P_{gIF} - A_{P_L}\ P_{LIF} = \frac{1}{12} M_P \ddot{x}_{P_F} - B \dot{x}_{P_F}$

35. $\dot{w}_{IF} = \frac{A_{PL}}{1728}\ \rho_F \dot{x}_{PF}$

36. $\dot{P}_{gIF} = \frac{\beta}{V_{LIF}} (\dot{w}_{IF} - \dot{w}_{FL})$

37. $V_{LIF} = V_{LIF\ (Final)} - V_{LIF(O)} - \frac{A_{PL}}{1728} x_{PF}$

38. $P_{LIF} - P_{FTCV} = \frac{C_{IF}}{\rho_F} \dot{w}_{FL}^2 + \frac{\ell}{gA} \ddot{w}_{FL}$

39. $\dot{P}_{FTCV} = \frac{\beta}{V_{FTCV}} (\dot{w}_{FL} - \dot{w}_{FPC} - \dot{w}_{FSC} - \dot{w}_{FD})$

40. $P_{FSTCV} = P_{FTCV} - \frac{C_7}{\rho_F} \dot{w}_{FSC}^2$

41. $P_{FPTCV} = P_{FTCV} - \frac{C_8}{\rho_F} (\dot{w}_{FPC} + \dot{w}_{FD})^2$

42. $\dot{w}_{FSC} = \frac{C_{V_{FSTCV}}}{56.8} \sqrt{\rho_F (P_{FSTCV} - P_{FJSC-U})}$

43. $\dot{w}_{FPC} = \frac{C_{V_{FPTCV}}}{56.8} \sqrt{\rho_F (P_{FPTCV} - P_{FJPC-U})}$

44. $\dot{w}_{FD} = \frac{C_{V_{FDV}}}{56.8} \sqrt{\rho_F P_{FPTCV}}$

45. $P_{FJSC} = P_{FJSC-U} - \frac{C_9}{\rho_F} \dot{w}_{FSC}^2$

46. $P_{FJPC} = P_{FJPC-U} - \frac{C_{10}}{\rho_F} \dot{w}_{FPC}^2$

47. $P_{FJSC-U} = P_{CSC} + \frac{C_9 + C_{11}}{\rho_F} \dot{w}_{FSC}^2$

48. $P_{FJPC-U} = P_{CPC} + \frac{C_{10} + C_{12}}{\rho_F} \dot{w}_{FPC}^2$

49. $\dot{w}_{TP} = \dot{w}_{OPC} + \dot{w}_{FPC}$

50. $\dot{w}_{TS} = \dot{w}_{OPC} + \dot{w}_{FPC} + \dot{w}_{OSC} + \dot{w}_{FSC}$

51. $\dot{P}_{CPC} = \frac{R_P\ T_P}{144\ V_{PC}} (\dot{w}_{TP} - \frac{gA_{t_P} P_{CPC}}{C^*_P})$

52. $\dot{P}_{CSC} = \frac{R_S\ T_S}{144\ V_{SC}} (\dot{w}_{TS} - g \frac{gA_{t_S} P_{CSC}}{C^*_S})$

where:

the dot ($\cdot$) convention represents the first derivitive and

A = area in ft^2

c = flow resistance in psi $sec^2/lb\ ft^3$

ΔF = differential force in lbs

g = acceleration of gravity = 32.2 ft/sec^2

k = Smith's constant

ℓ = pipe distance in feet

M = mass in lb sec^2/ft

N = the flow factor and is a nondimensional function of Mach number

R = the gas constant = 1544/gas molecular weight = 55 for N_2

T = absolute temperature in ^oR

T_T = total temperature in ^oR

V = volume in ft^3

W = total mass in lbs

$\dot{w}$ = flow rate in lbs/sec

x = position in inches

β = compressibility effects in psi ft^3/lb

ρ = density in lb/ft^3

Subscripts consist of:

B = bottle

D = dump

F = fuel

g = gas

J = injector

JPC-U = upstream of primary combustor injector

JSC-U = upstream of secondary combustor injector

L = line

O = oxidizer

P = piston

P, PC = primary combustor

PRV = pressure regulator (control) valve

PTCV = primary thrust chamber valve

S, SC = secondary combustor

STCV = secondary thrust chamber valve

T = total

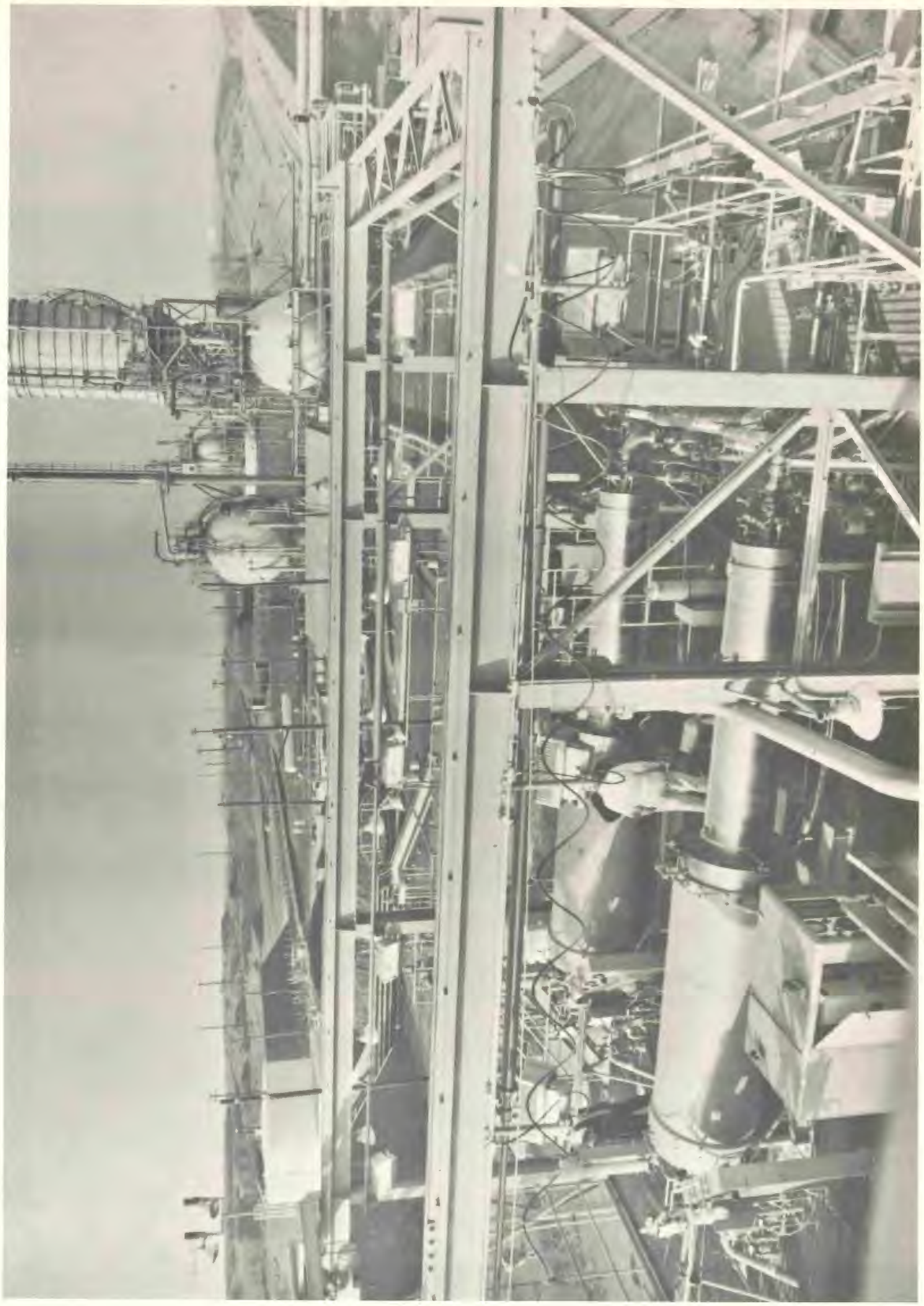

FIG. 1. PROPELLANT INTENSIFIER -- SIDE VIEW

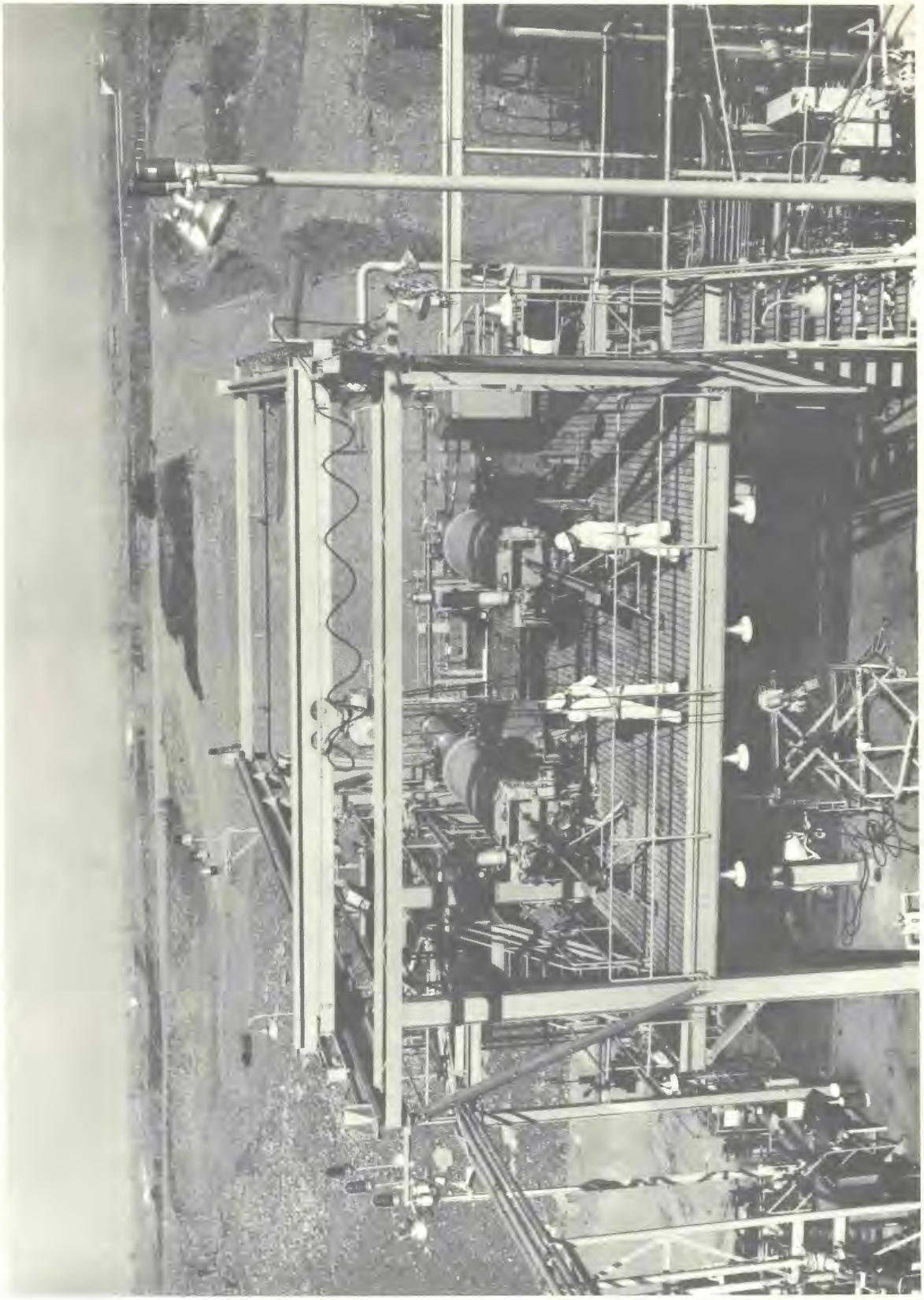

FIG. 2. PROPELLANT INTENSIFIER -- AFT VIEW

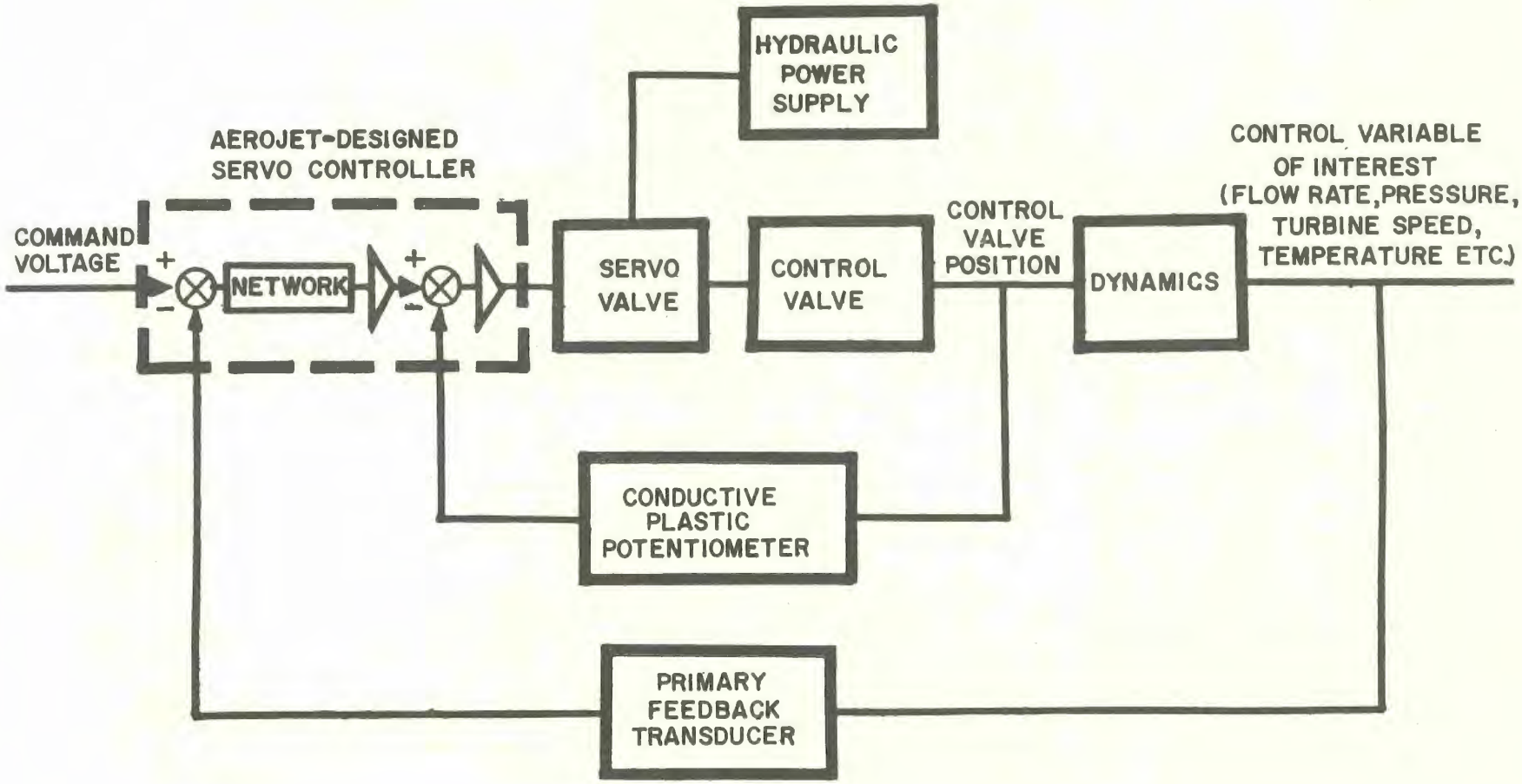

FIG. 3. BASIC CLOSED-LOOP CONTROL SUBSYSTEM CONFIGURATION

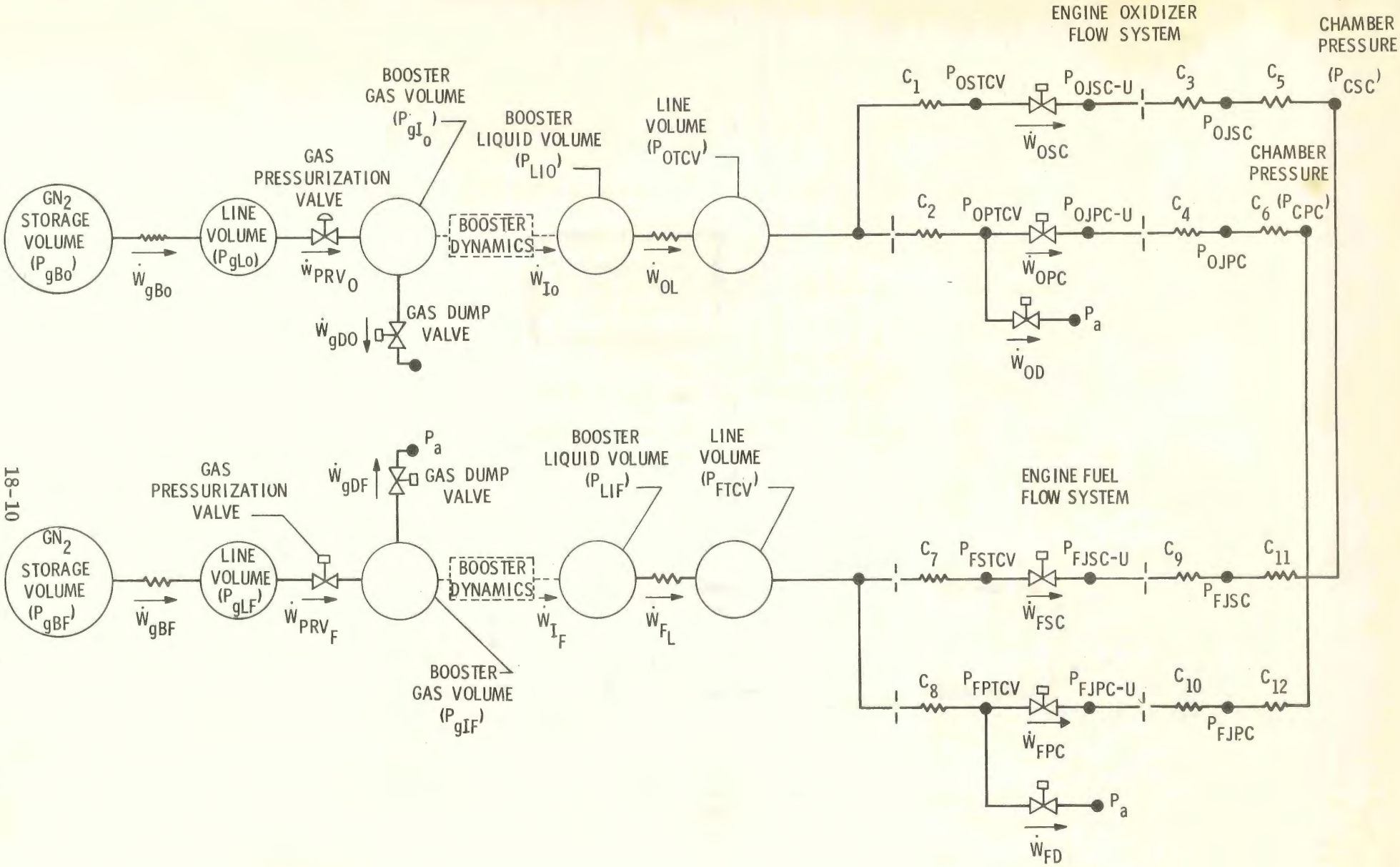

FIG.4. FUNCTIONAL FLOW DIAGRAM FOR PROPELLANT INTENSIFIER SYSTEM

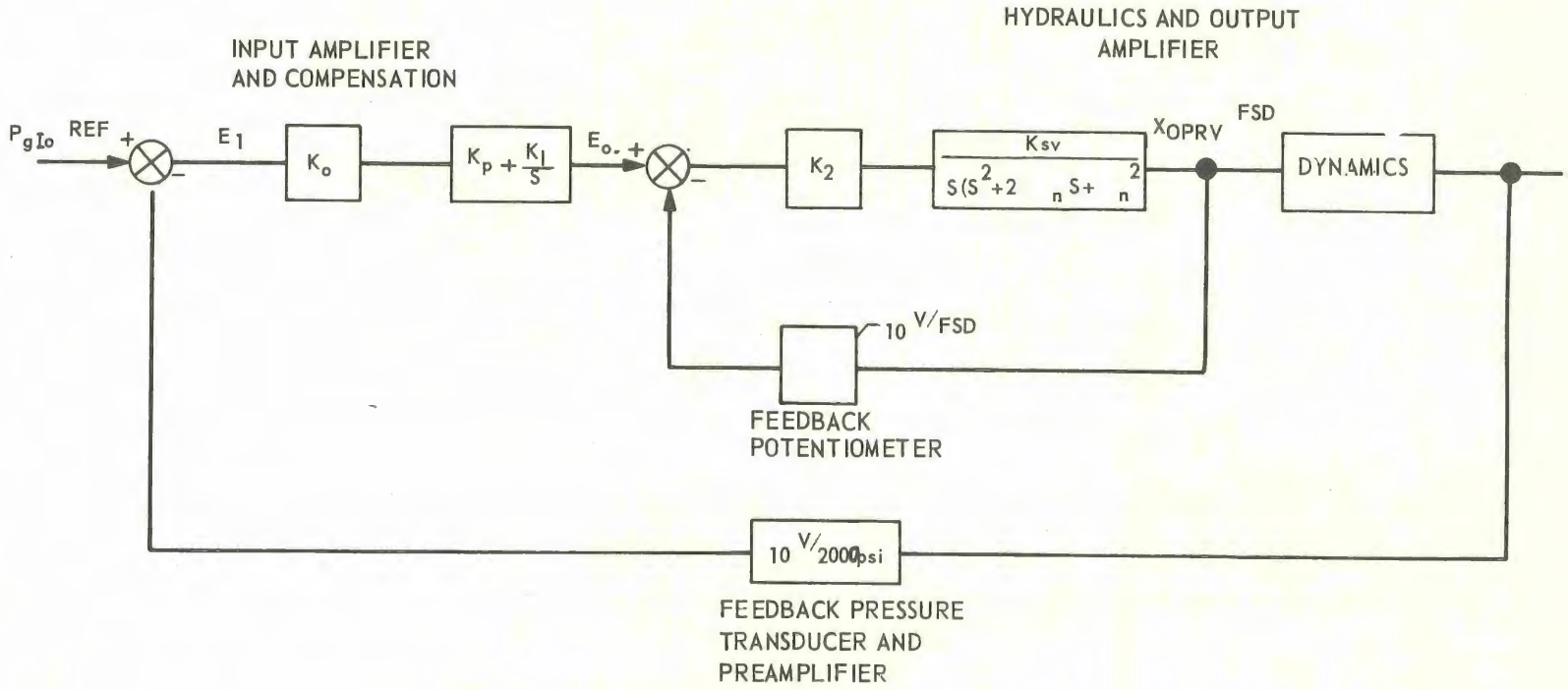

FIG.5. FUNCTIONAL BLOCK DIAGRAM FOR OXIDIZER INTENSIFIER SERVO SUB-SYSTEM

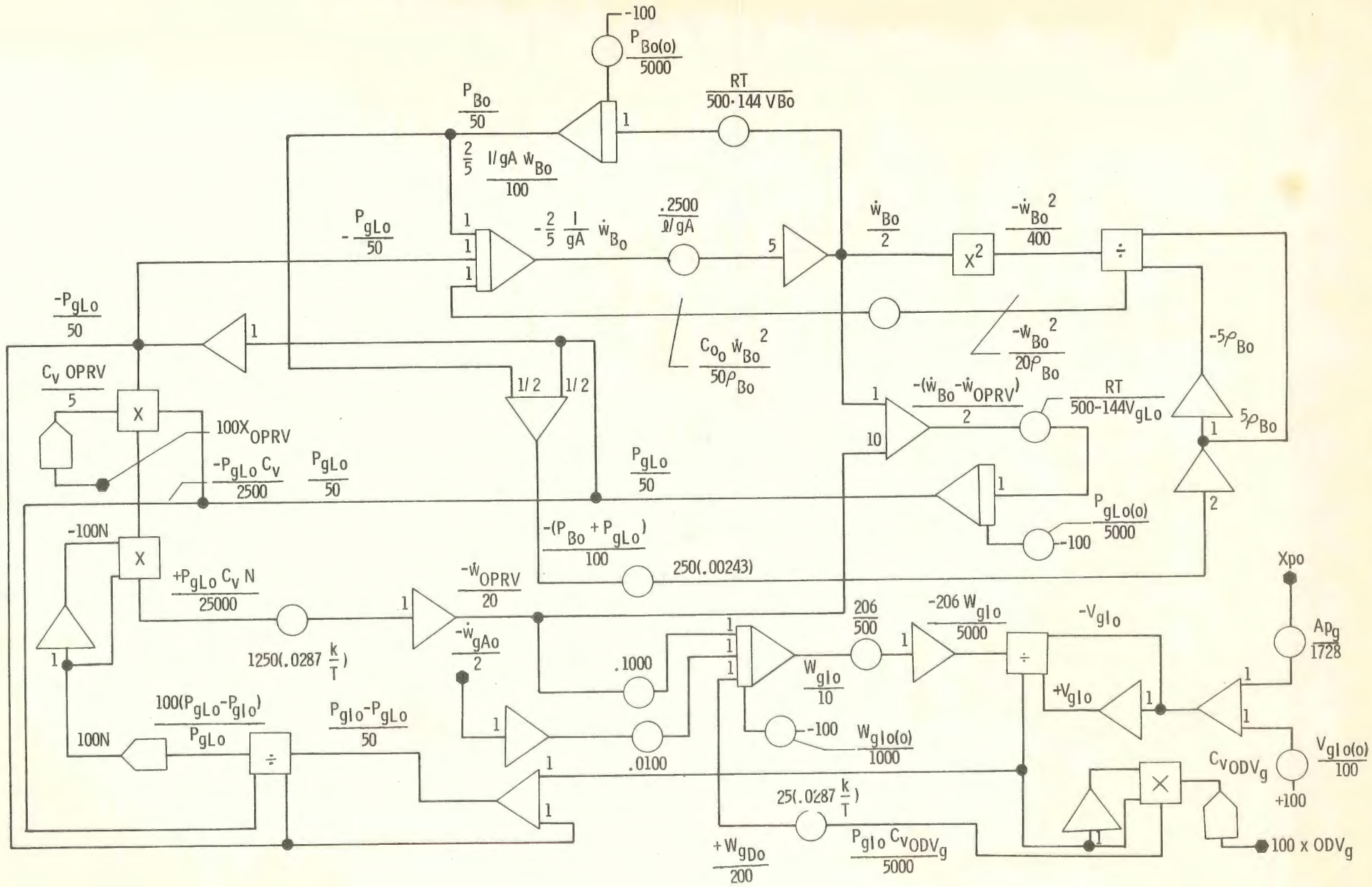

FIG.6. OXIDIZER GAS-SIDE ANALOG COMPUTER SIMULATION DIAGRAM

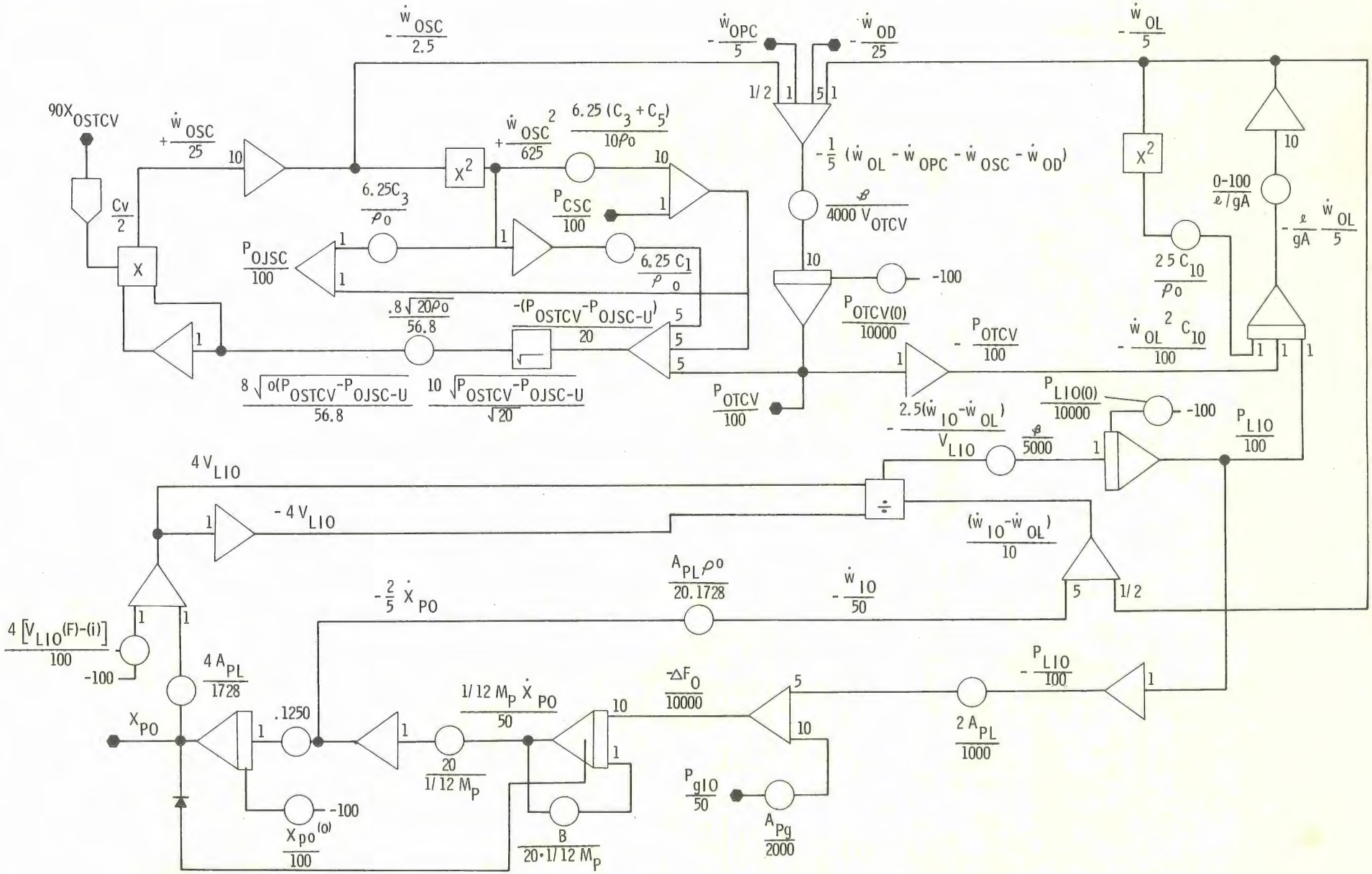

FIG.7. OXIDIZER LIQUID DYNAMICS AND SECONDARY COMBUSTOR SIMULATION DIAGRAM

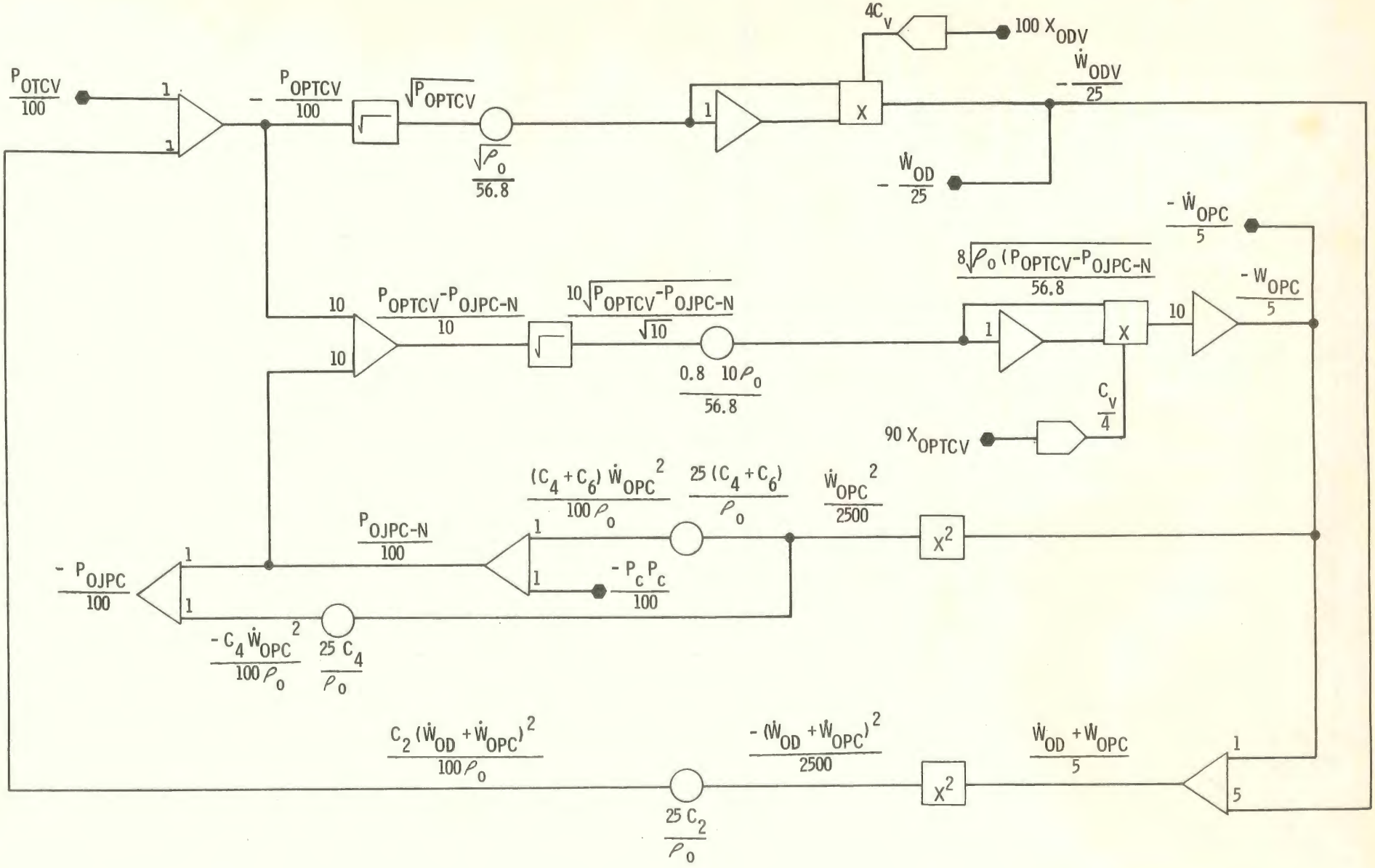

FIG.8. OXIDIZER PRIMARY COMBUSTOR COMPUTER SIMULATION DIAGRAM

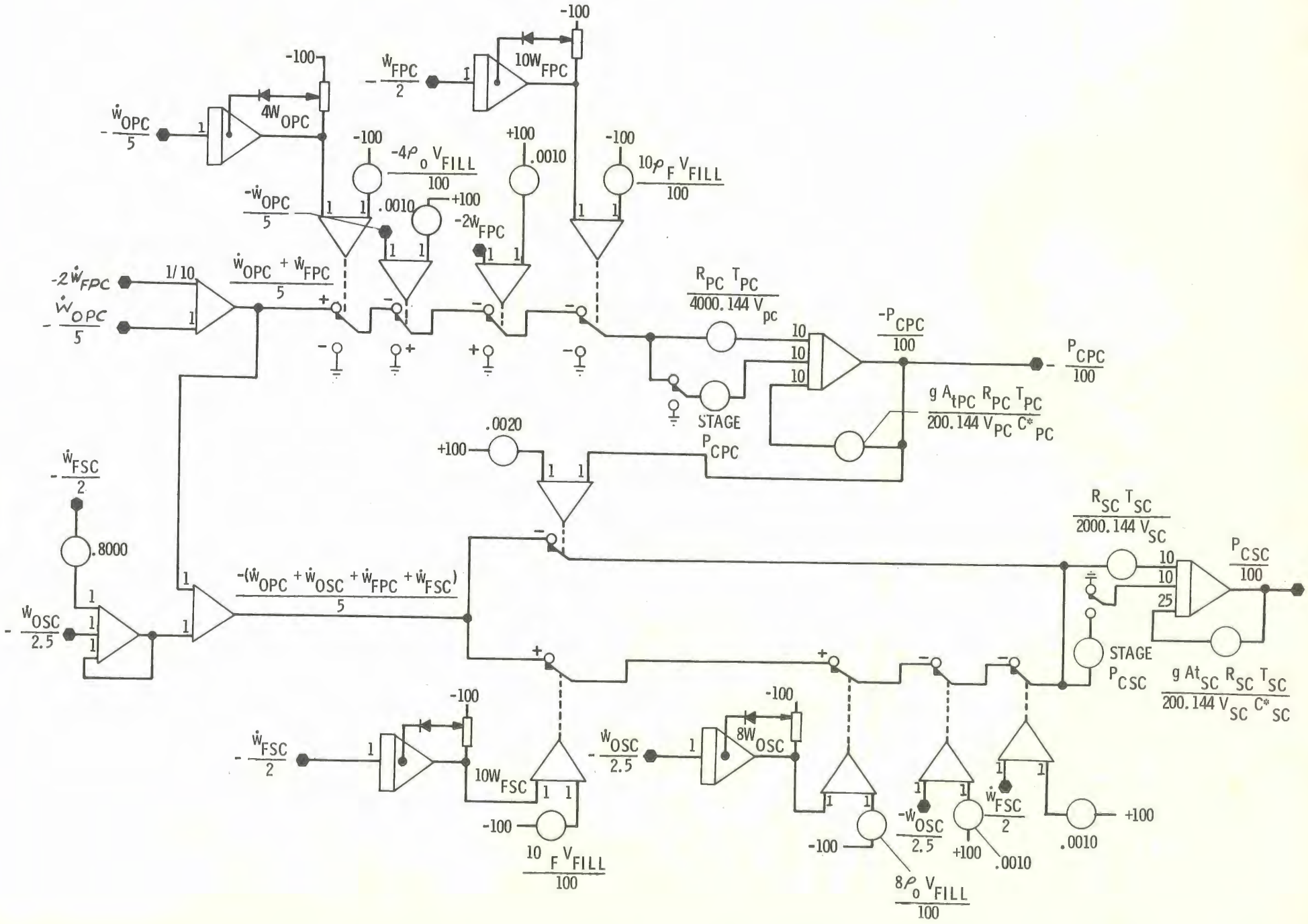

FIG.9. CHAMBER PRESSURE COMPUTATIONAL SIMULATION DIAGRAM

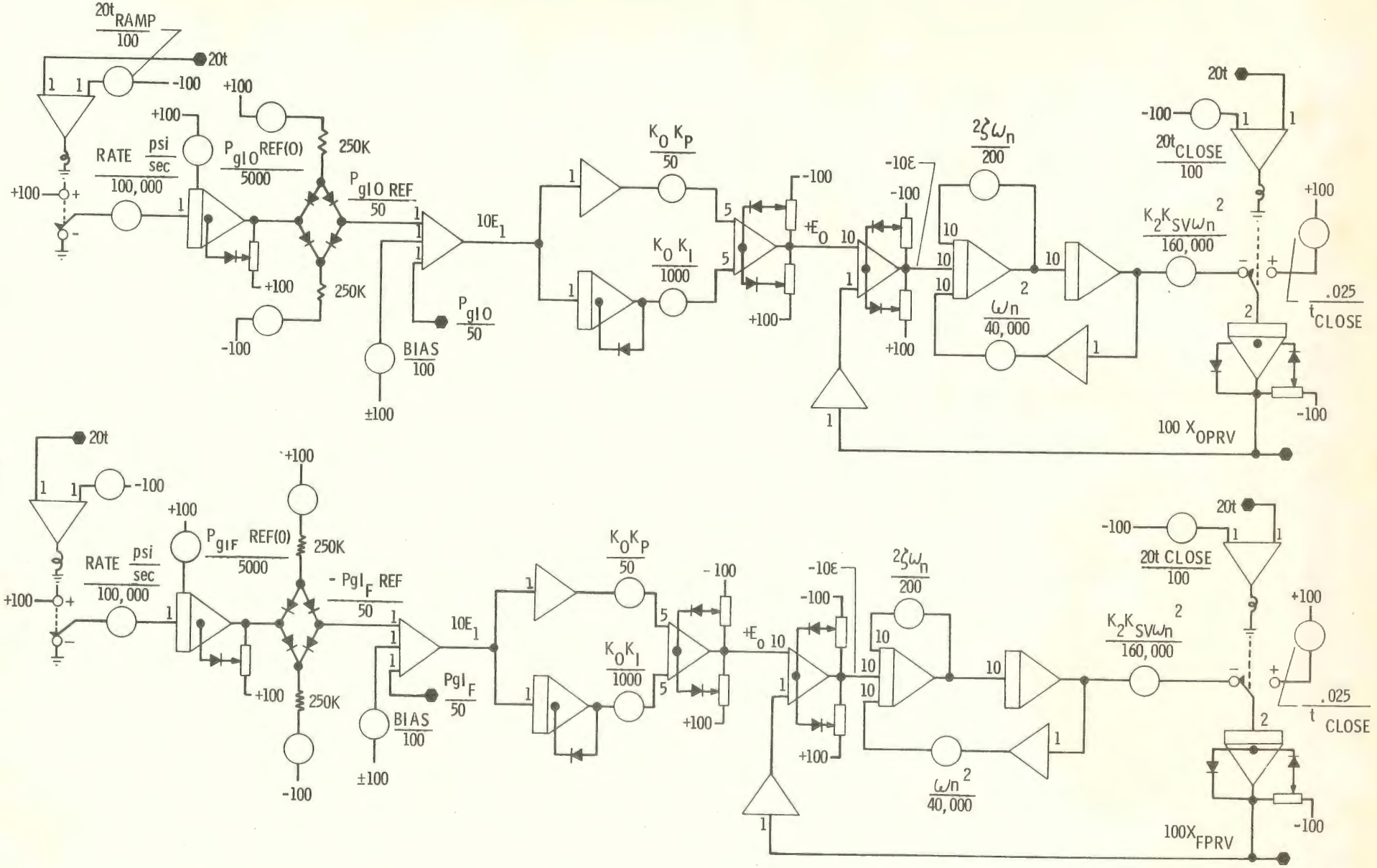

FIG.10. GAS VALVE CONTROL SUB-SYSTEM COMPUTER SIMULATION DIAGRAM

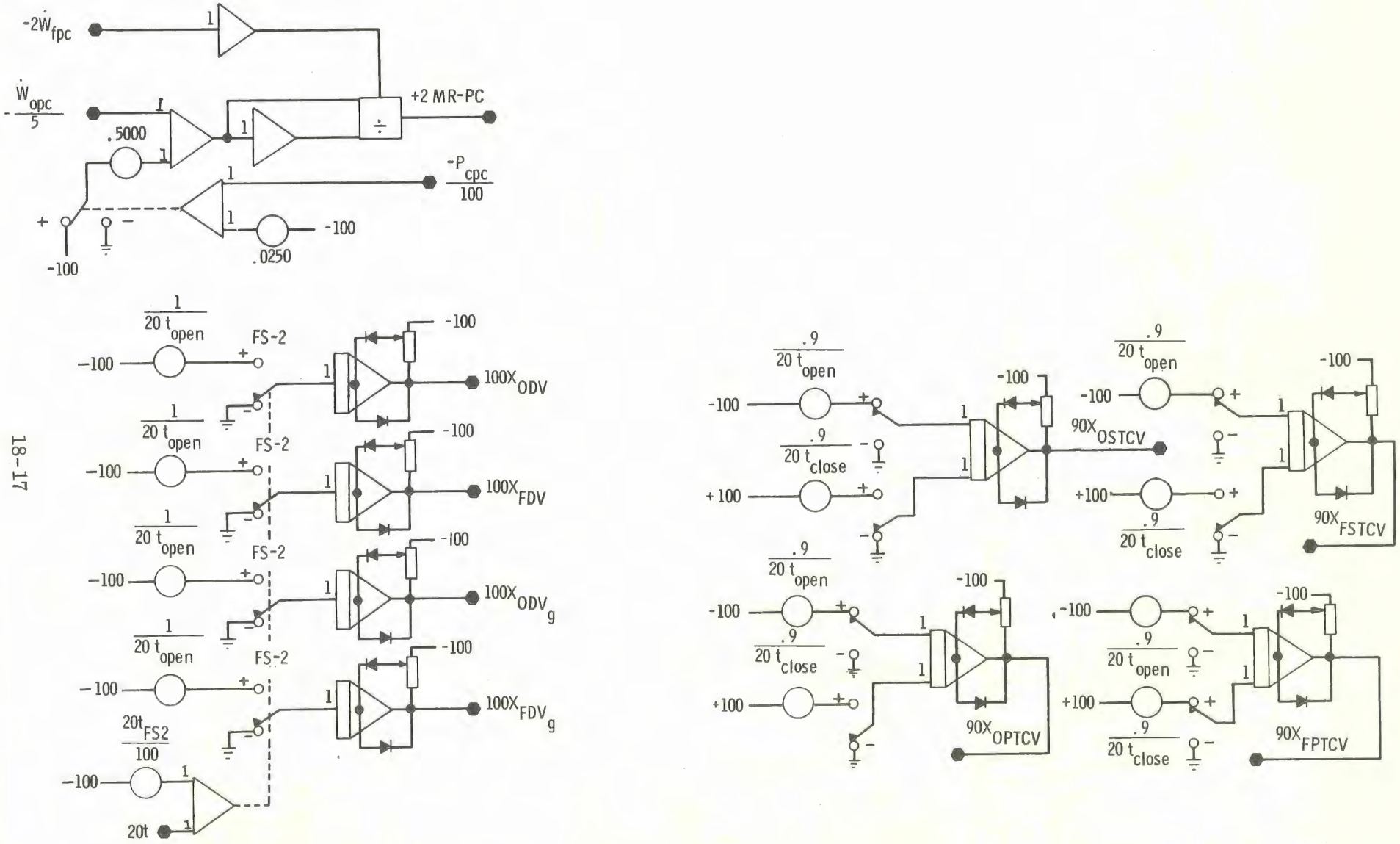

FIG.11. DUMP VALVE AND THRUST CHAMBER VALVE COMPUTER SIMULATION DIAGRAM

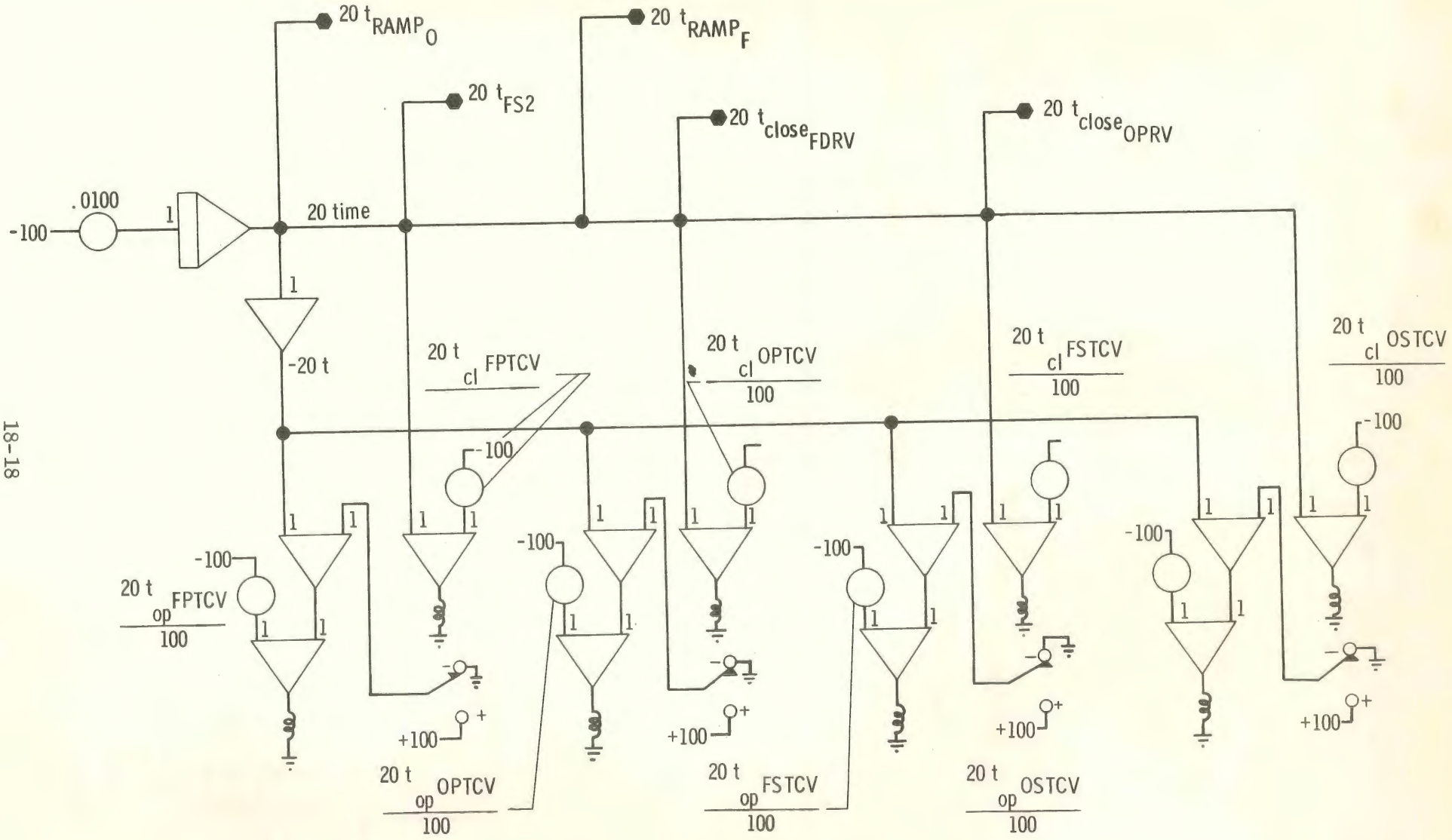

FIG. 12. ANALOG COMPUTER LOGIC DIAGRAM

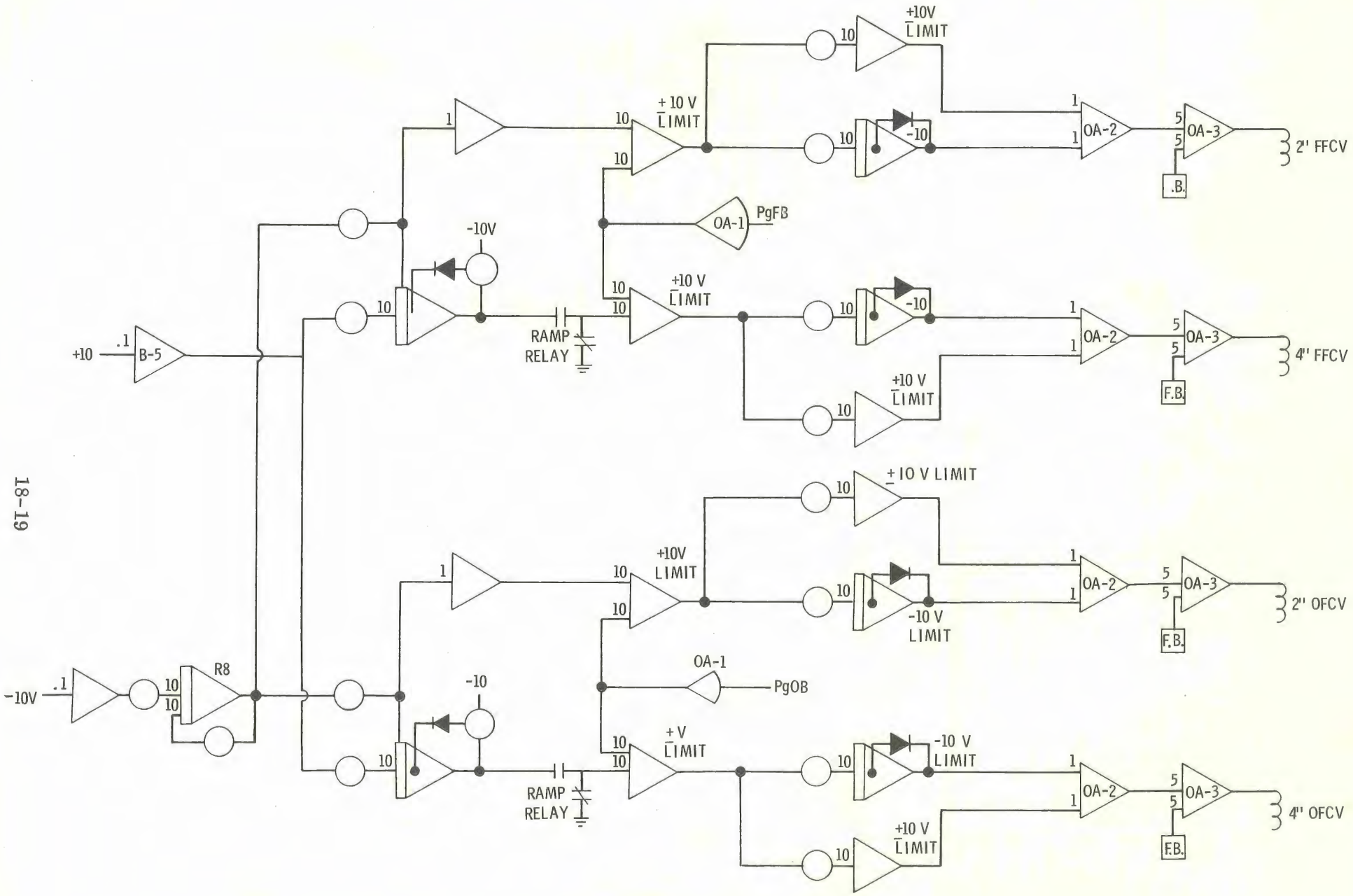

FIG.13. ON-LINE ANALOG COMPUTER PROGRAM

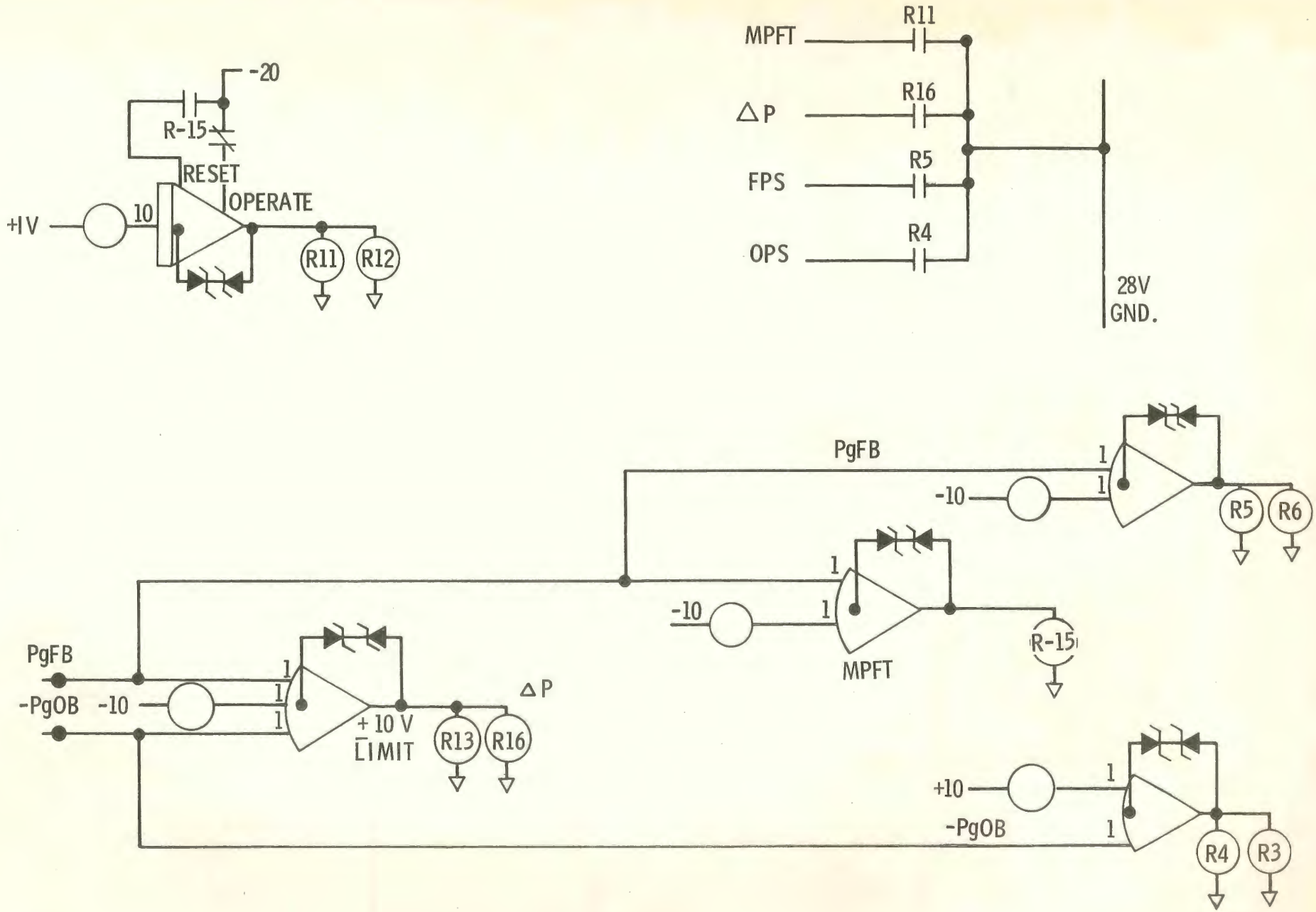

FIG. 14. COMPUTER FAIL-SAFE SHUTDOWN CIRCUITRY

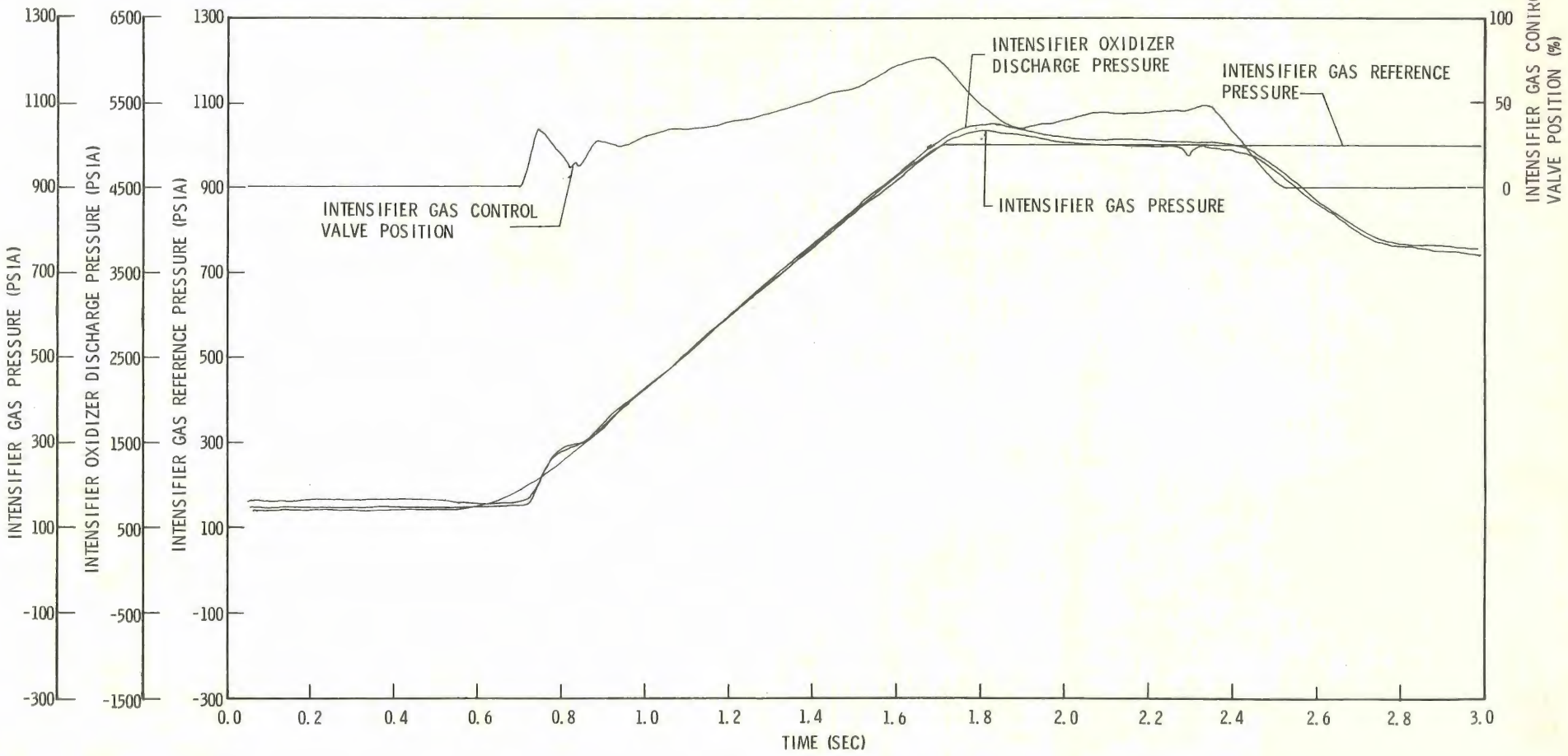

FIG. 15. TYPICAL OXIDIZER INTENSIFIER OPERATIONAL DATA

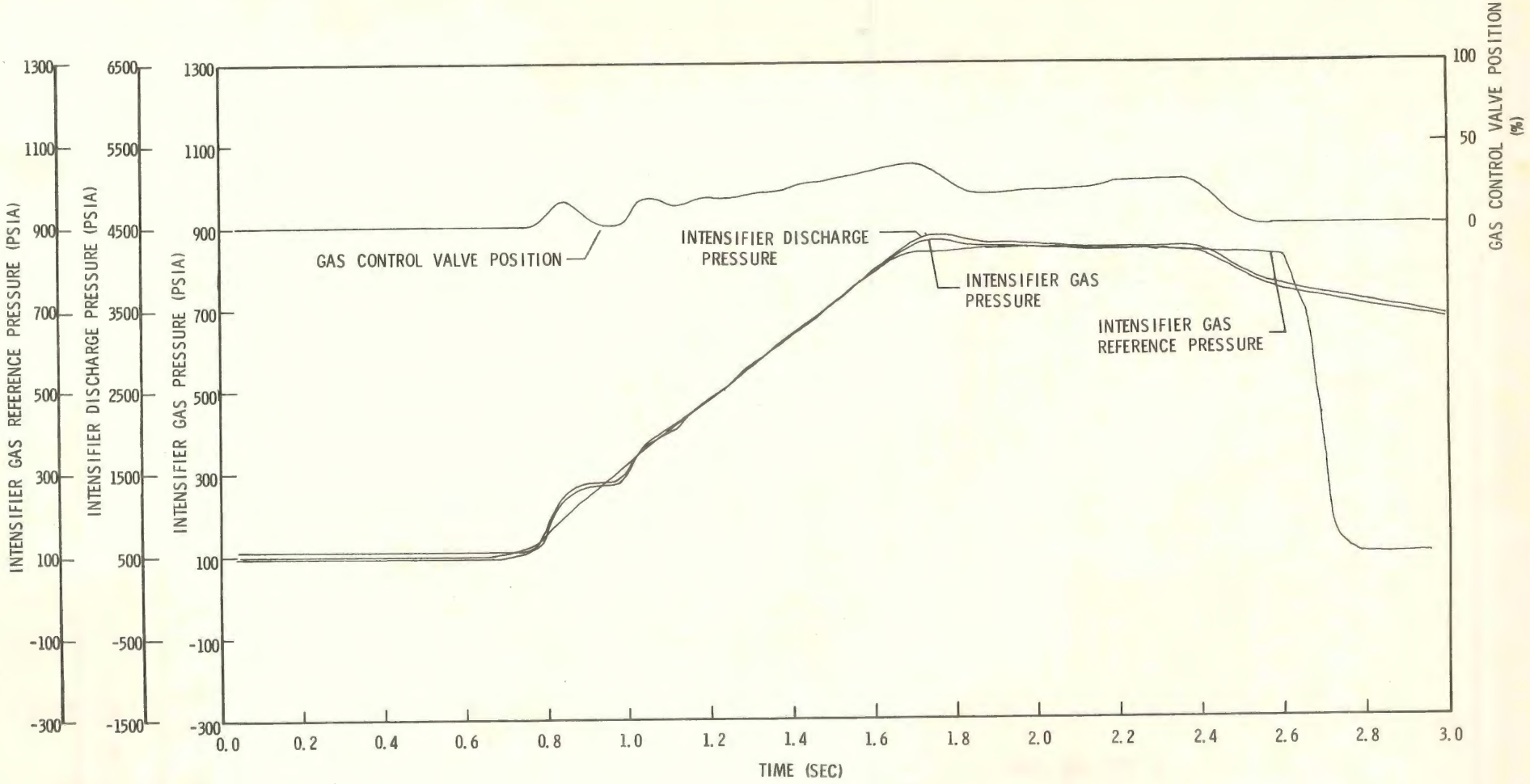

FIG.16. TYPICAL FUEL INTENSIFIER OPERATIONAL DATA

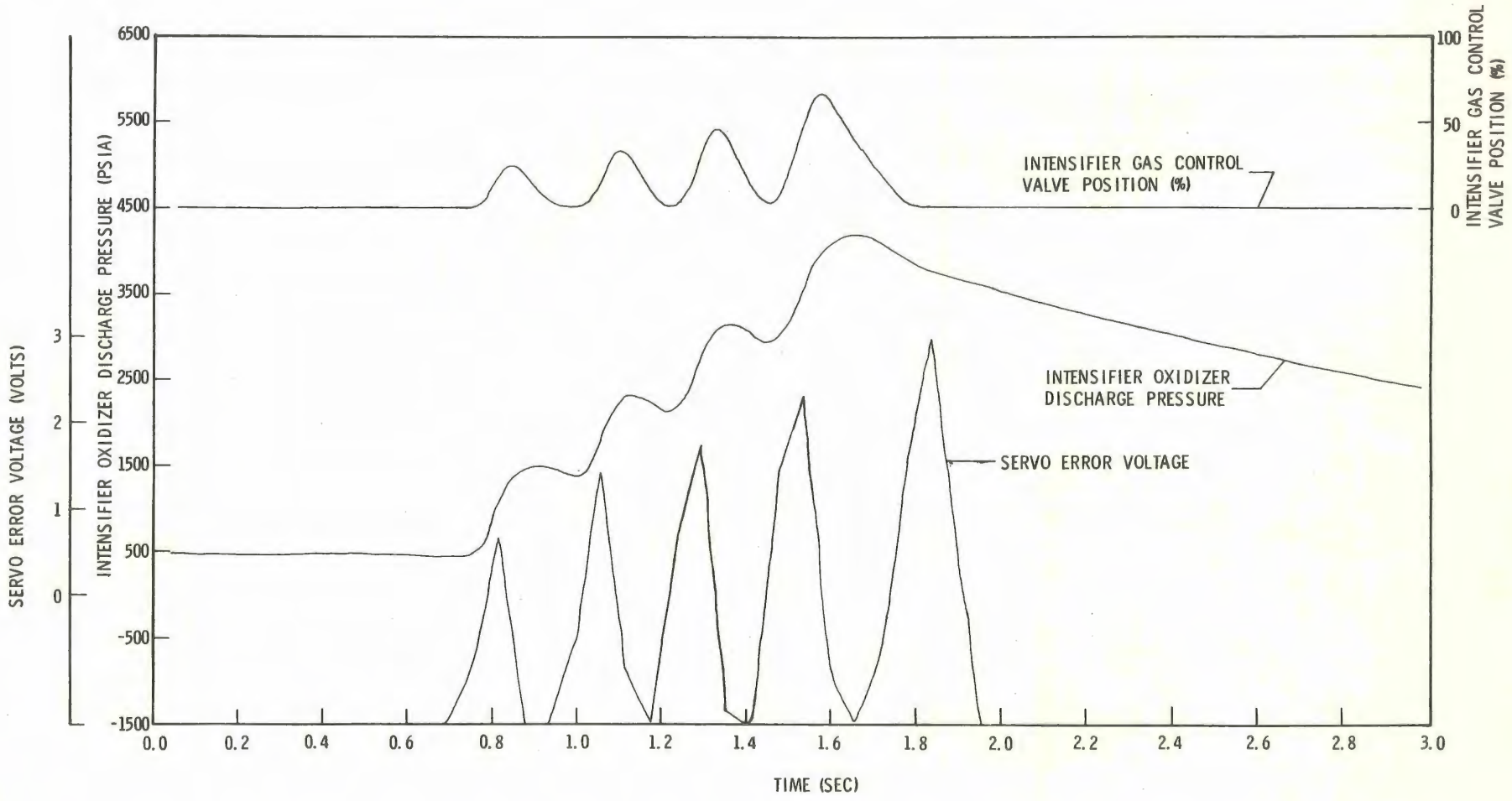

FIG.17. RESULTS OF IMPLEMENTING INCORRECT SERVO SUB-SYSTEM GAIN